Binary Plankton Image Classification

Xiaoou Tang, *Senior Member, IEEE*, Feng Lin, Scott Samson, and Andrew Remsen

***Abstract*—In marine biology study, it is important to investigate the distribution of plankton organisms. Because of the overwhelming data size, automatic processing of the large amount of image data collected by underwater image recorders becomes inevitable. However, due to the fragmentation and the large within-class variations of binary plankton images, it is difficult to extract reliable shape features. In this paper, we propose several new shape descriptors and use a normalized multilevel dominant eigenvector estimation method to select a best feature set for binary plankton image classification. We achieve more than 91% classification accuracy in experiments on more than 3000 images.**

***Index Terms*—Binary plankton images, feature extraction, principal component analysis (PCA), two-dimensional (2-D) shape recognition.**

I. Introduction

PLANKTON form probably the most important component of the ocean food web. It includes both the phytoplankton (all kinds of drifting plants and bacteria) and the zooplankton (animal plankton). Because of their ability to rapidly respond to environmental changes such as eutrophication or pollution, plankton are often regarded as indicators of aquatic health. Therefore, it is important for oceanographic researchers to study the temporal variation and spatial variability in plankton abundance and distribution. In the past, investigators were limited to collecting plankton samples using methods such as towed nets, pumps, and Niskin bottles, and then manually counting and identifying the organisms in each sample. Given the large number of samples that are collected during a cruise, this can be prohibitively expensive and time consuming. To improve sampling efficiency, some underwater imaging sensors such as the video plankton recorder [1], the HOLOMAR underwater holographic camera system [2], [3], and the shadowed image particle profiling and evaluation recorder (SIPPER) [4] have been developed to continuously capture magnified plankton images *in situ*. By applying the computer vision technique to rapidly recognize plankton images, the real-time analysis of plankton population dynamics becomes possible [5], [20].

In this paper, we develop several new features for binary plankton classification. To effectively combine the new features with traditional shape features and produce a compact feature vector for classification, we need an effective feature selection algorithm. Although different features may be successful at different aspects because of the different techniques, they are all based on the same object shape. Therefore, it is inevitable for these features to contain overlapping information. The principal component analysis (PCA) is a powerful feature reduction and selection tool. Its decorrelation ability serves to decorrelate redundant features, and its energy packing property serves to compact useful information into a few dominant features.

However, simply using the PCA on a large feature vector combining all the individual feature vectors may not work. In addition to the expensive computational requirement, many small feature vectors of small dimensions and scales will be overwhelmed by other large feature vectors even though the small features may contain discriminating information. In this paper we propose a normalized multilevel dominant eigenvector estimation (NMDEE) method based on the multilevel dominant eigenvector estimation (MDEE) method we developed in [14] to combine feature vectors for plankton recognition. The method reduces computational complexity by several orders of magnitude over a standard PCA and achieves a much better feature extraction performance.

The plankton classification system was tested on seven classes of more than 3000 plankton images. The experimental results demonstrate that the features extracted by the normalized MDEE performed significantly better than those by the conventional PCA and a classification accuracy of 91.70% was achieved, making it comparable to the accuracy by the laborious manual classification method [15].

II. Methodology

A. Fourier Descriptor

Fourier descriptors (FDs) have been used as shape features in a number of applications [6]–[10]. For a closed boundary defined by a closed sequence of successive boundary pixel coordinates, the centroidal radius function is the distance from the boundary points to the centroid of the object. The FD is defined as a normalized discrete Fourier transform of the radius boundary function. Since the FD features are computed around the centroid of the object, they are translation invariant. The rotation and scale invariance of the feature vector can be derived from the shift invariant and linear properties of the DFT magnitudes.

B. Moment Invariants

The moment invariants are computed from algebraic invariants of rigid objects [11]–[13]. Their generating function is

$$M(u,v) = \int\int e^{ux+vy} f(x,y)dxdy. \tag{1}$$

Manuscript received May 6, 2003; accepted January 8, 2004. This work was supported in part by the Research Grants Council of the Hong Kong Special Administrative Region and by the Office of Naval Research under Grants N00014-02-1-0266 and N00014-96-1-5020. **Associate Editor: A. Trucco**.

X. Tang and F. Lin are with the Department of Information Engineering, The Chinese University of Hong Kong, Shatin, Hong Kong (e-mail: xtang@ie.cuhk.edu.hk).

S. Samson is with the Center for Ocean Technology, University of South Florida, Tampa, FL 33620 USA.

A. Remsen is with the College of Marine Science, University of South Florida, Tampa, FL 33620 USA.

Digital Object Identifier 10.1109/JOE.2004.836995

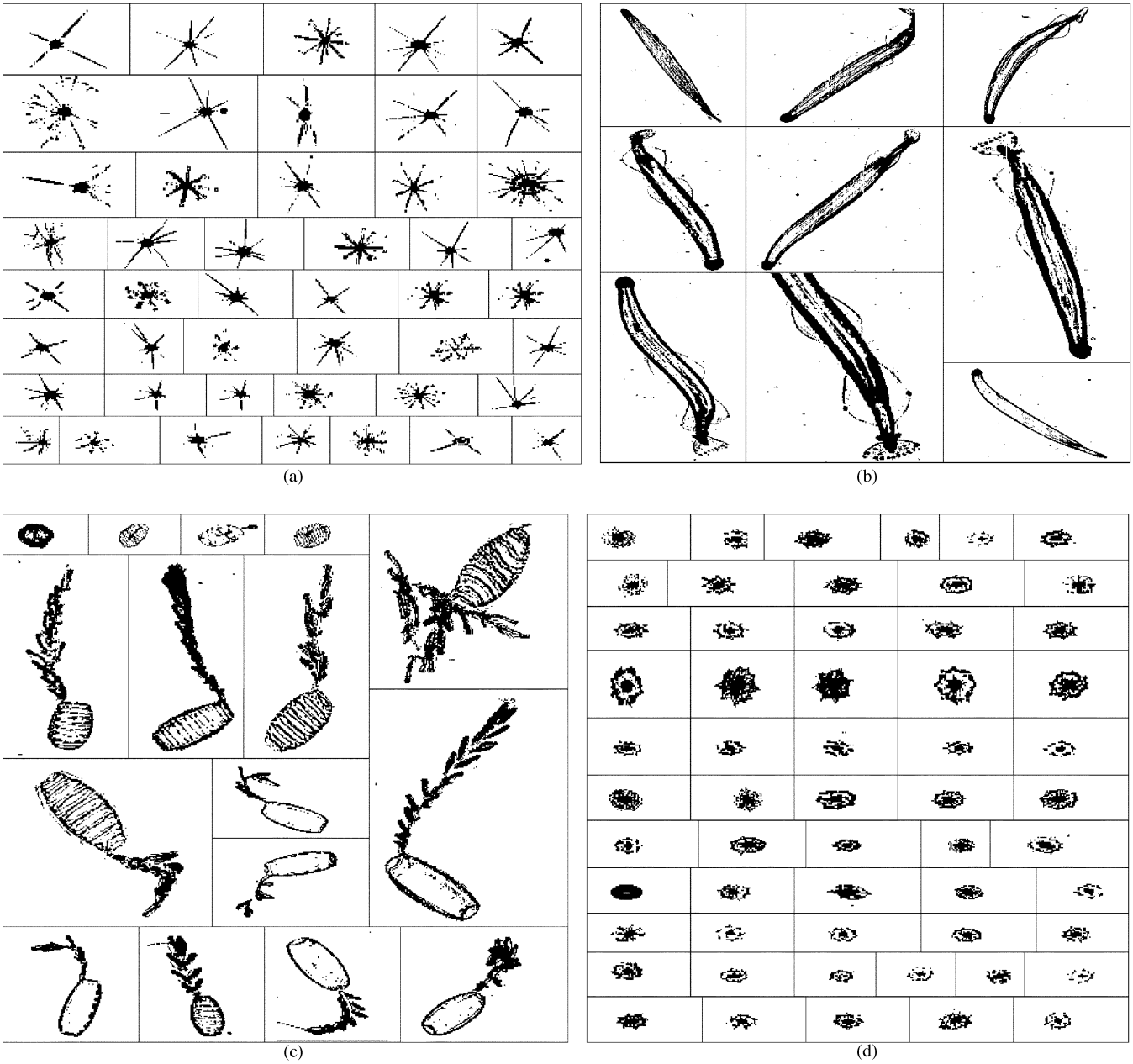

Fig. 1. Sample plankton images in seven classes. (a) Class 1: Acantharia. (b) Class 2: Chaetognath. (c) Class 3: Doliolid. (d) Class 4: Radiolaria.

Based on methods of algebraic invariants, invariant moments are computed using nonlinear combinations of the second and third normalized central moments. These invariant moments possess the translation, rotation, and scale invariant properties. However, since our study objects are the images of nonrigid plankton organism, moment invariants may not perform well.

C. Granulometry

Granulometry is defined to extract size distributions in binary images [16]–[18]. By performing a series of morphological openings of increasing kernel sizes, we can obtain the granulometry function that maps each kernel size to the number of image pixels removed during the opening operation with the corresponding kernel.

Consider two subsets in two-dimensional (2-D) Euclidean space, T and G. The opening of G by T is defined by [19]

$$G \circ T = \cup\{T + x : T + x \subset G\} \tag{2}$$

where $T+x$ is the translation of T at x. Then, the granulometric size distribution of G is given by

$$F_G(\lambda) = 1 - \frac{\nu(\Psi_\lambda(G))}{\nu(G)} \tag{3}$$

where ν denotes the area and $\Psi_\lambda(G) = G \circ \lambda T$. T can be any convex and compact set including the origin, and λT is a family of structuring elements of increasing size. Thus the multiscale

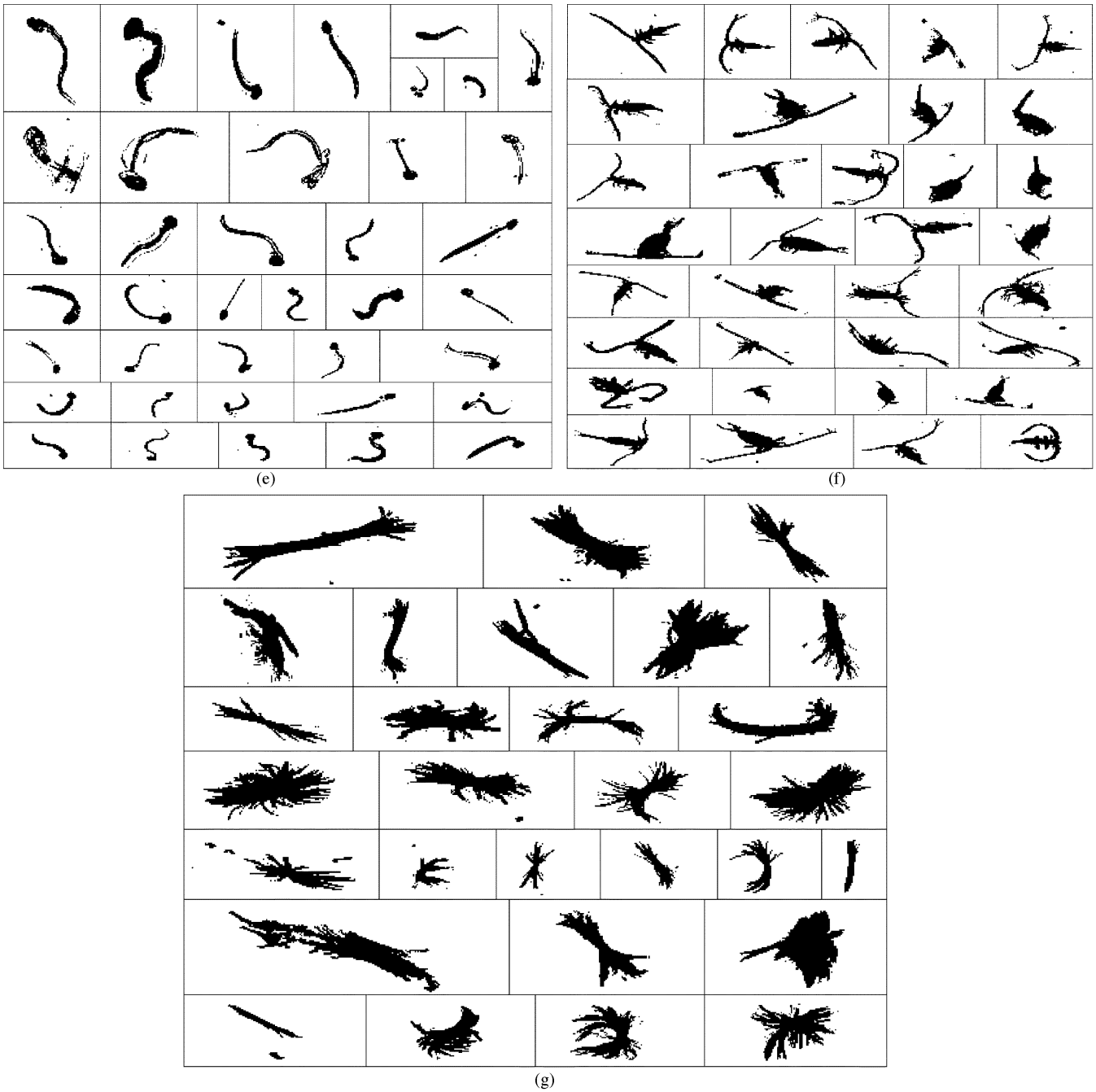

Fig. 1. *(Continued.)* Sample plankton images in seven classes. (e) Class 5: Larvaceans. (f) Class 6: Calanoid. (g) Class 7: Trichodesmium.

shape feature of a binary image can be described by the granulometry.

D. Circular Projection

To characterize the linear shapes in plankton objects, we propose a circular projection feature vector. We first project the binary object in the horizontal direction, and then find the maximum value of the projection. This value should reflect the longest linear structure in the vertical direction of the object. For example, if we only have a vertical line in the object, then only one large nonzero value exists in the projection in the horizontal direction.

If we project the object in all directions and select the largest value M_i in each projection, we get a feature vector

$$CM = [M_1, \ldots, M_N] \tag{4}$$

where N is the number of directions we conduct the projection. If $M_p = \max\{M_i, i = 1, 2, \ldots, N\}$, the most significant linear feature of object will appear at direction p. Obviously, CM is translation invariant. To achieve the scale and rotation invariance, CM is normalized and circularly shifted with respect to the M_p to get

$$CMS = \left[\frac{M_p}{S}, \ldots, \frac{M_N}{S}, \frac{M_1}{S}, \ldots, \frac{M_{p-1}}{S}\right] \tag{5}$$

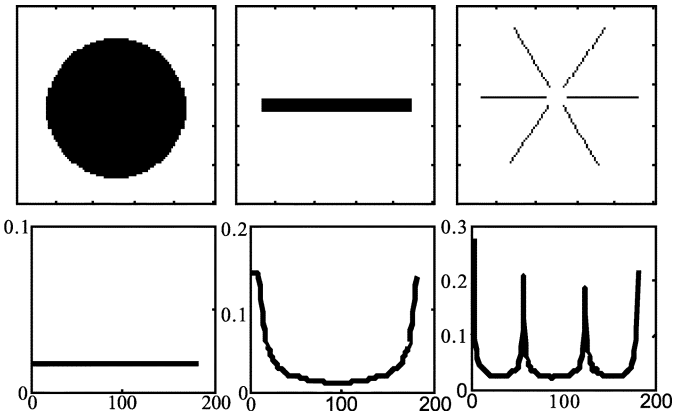

Fig. 2. Shape examples and their CMS.

where S is the area of the object. Some example objects and their CMS are depicted in Fig. 2, which are the simplified prototypes of class Radiolaria, Chaetognath, and Acantharia, respectively. The data in this paper come from the SIPPER system developed by University of South Florida, which is equipped with a laser imaging source and a fast high-resolution line-scan camera to continuously take binary pictures of a 10 cm $\times$ 10 cm area when moving though the water. Some examples are shown in Fig. 1. The objects are fairly noisy, fragmental, and nonrigid in shape, thus features derived from the boundary descriptors [6]–[10] and invariance moments [11]–[13] may not work well. Especially, the features we used for gray-scale plankton image recognition [5] are no longer sufficient for the binary plankton images. New shape features are needed to distinguish the different plankton categories.

To describe the shape in more detail, the entire projection vector in the p direction and its orthogonal direction are also used as feature vectors. They are called the feature vector $P1$ and $P2$, respectively.

E. Smoothness of Kernel Boundary

Plankton such as Larvaceans, tend to have a smooth kernel portion with a long tail. It is difficult to use FD to measure the smoothness of the whole object since the smooth portion and the tail portion will be averaged together. We propose a smoothness measure that only works on the body kernel.

We first developed an algorithm to extract the kernel section from its narrow neck portion by the morphological operations, as illustrated in Fig. 3. We apply a flood fill operation to fill all the internal holes of the binary object. Then a sequence of opening operations are only applied to the side with the tail attached, to remove the tail without affecting the smoothness of the kernel much.

To evaluate the smoothness of the extracted kernel boundary, we use the following measure:

$$M_\lambda = \frac{\frac{P^2}{A}}{\frac{\pi(\lambda+1)^2}{\lambda}} \tag{6}$$

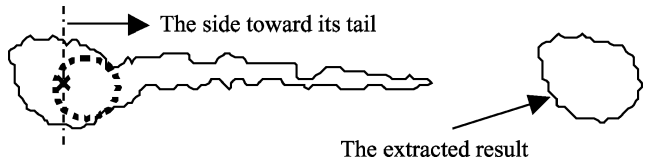

Fig. 3. Boundary of a Larvacean image, where the centroid of its kernel section is denoted by "x," and the dotted circle is the opening kernel.

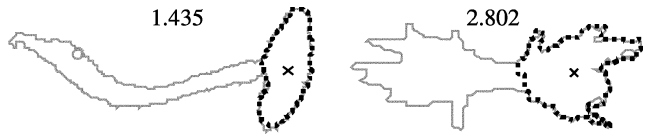

Fig. 4. Two results (marked by dotted lines in their original object boundaries) with their smoothness values, where the left one is a Larvacean and the right is the typical shape of a Trichodesmium.

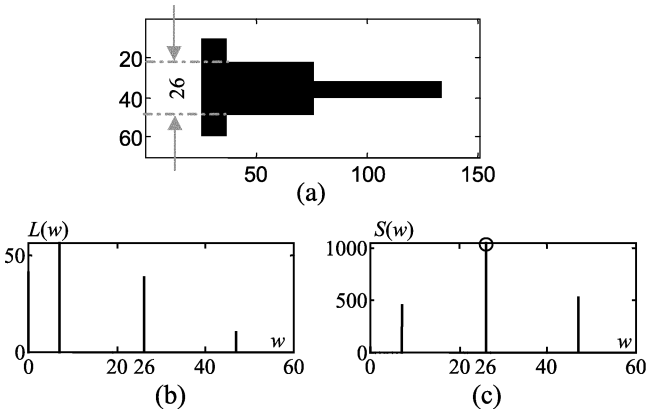

Fig. 5. Computation of the *dominant object pixel-width*. (a) Simple binary object. (b) Object *pixel-width* histogram of (a). (c) Area distribution of the object *pixel-width*, where $S(w) = L(w) \times w$. The w corresponding to the max $S(w)$ is the *dominant object pixel-width*, which is marked by "o" at $w = 26$.

where P and A are the perimeter and area of the object, $\lambda = (a/b)$ is the ratio of the length a and width b of the object's bonding box. If the boundary is a smooth close curve, we have $M_\lambda \to 1$. If and only if the boundary is an ellipse curve, we have $M_\lambda = 1$. Two examples of the extracted kernel boundary are shown in Fig. 4. The smoothness values of the two objects are significantly different.

F. Object Width and Density

Because of the diverse shapes of plankton, it is difficult to have a stable measure of the width of the plankton. We developed a novel dominant width measure that uniquely reflects the width of the dominant portion of the object.

We use a simple example in Fig. 5 to illustrate the computation of the dominant object *pixel-width*. The principle object direction is first rotated to the horizontal direction. The object *pixel-width* histogram $L(w)$ is then computed, as shown in Fig. 5(b), where the horizontal axis represents the pixel width w, and the vertical axis shows the length of all segments along the body principle axis that have the same width. The width w of the three peaks of $L(w)$ in Fig. 5(b) reflects the width of the

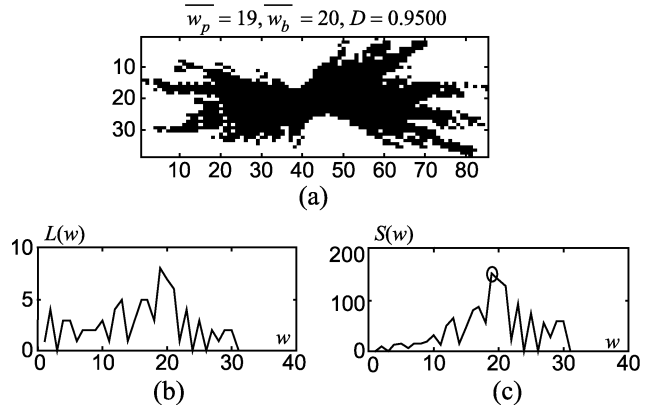

Fig. 6. Example of the *dominant object pixel-width*. (a) Binary rotated object with the horizontal axis corresponding to its principle direction. (b) Histogram of object *pixel-width*. (c) Area distribution of *object pixel-width*, where $S(w) = L(w) \times w$. The *dominant object pixel-width* is marked by "o" at $w = 19$.

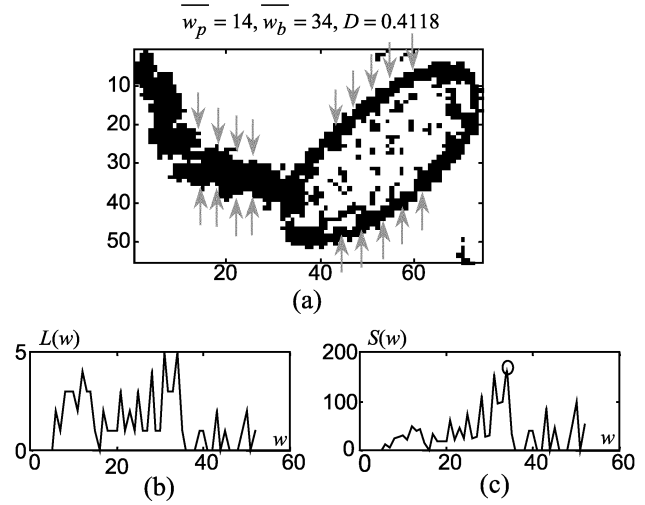

Fig. 7. Example of the *dominant object body-width*. (a) Binary rotated object, and the calculation of the *body-width* values is illustrated by the arrows. (b) Histogram of object *body-width*. (c) Area distribution of object *body-width*, where $S(w) = L(w) \times w$. The *dominant object body-width* is marked by "o" at $w = 34$.

three object parts. $L(w)$ can be regarded as the length of all segments consisting of the object profiles with width w, therefore, the area curve, $S(w) = L(w) \times w$ in Fig. 5(c) represents the area of these segments. The maximum point in $S(w)$ is the second point at $w = 26$, as shown in Fig. 5(c). It represents the area of the center portion of the object, which is the largest part in the object. We use the width of this dominant portion of the object as the *dominant object pixel-width* measure $\overline{w_p}$.

Fig. 6 shows an example of the computation of $\overline{w_p}$ for a Trichodesmium. For the *pixel-width* measure, we only consider the number of black pixels in the object. We can also compute the object *body-width* that describes the boundary width of the object, as depicted in Fig. 7(a) where a specimen of class Doliolid is used. An example for computing the *dominant object body-width* $\overline{w_b}$ is shown in Fig. 7(b) and (c).

The ratio of the two kinds of object width measures

$$D = \frac{\overline{w_p}}{\overline{w_b}} \tag{7}$$

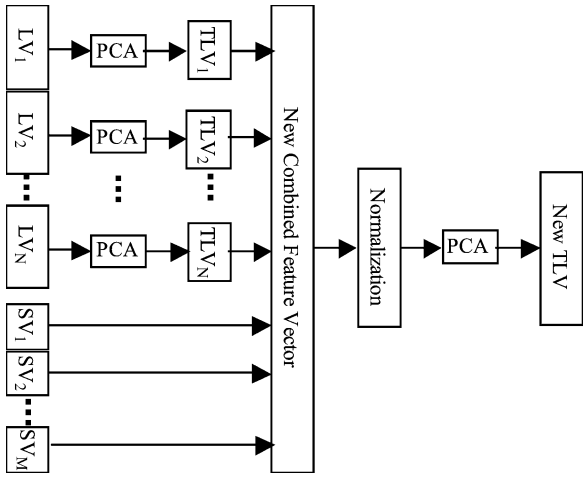

Fig. 8. Feature vector combination scheme, where LV represents the long feature vector, SV stands for the short feature vector, and TLV denotes the truncated vector selected by PCA.

reflects the density of the binary object, which is also a useful measure for the plankton objects. For example, the density of class Trichodesmium is dense, whereas that of class Doliolid is sparse, therefore, their measurements D as depicted in Figs. 6(a) and 7(a) are very different.

G. Feature Combination and Normalization

The features we extracted contain some long feature vectors (LV) such as FD, CMS, $P1$, and $P2$, and some short simple feature vectors (SV) such as Granulometry, moment invariants, boundary smoothness, object density, and some other simple shape features. There exists much redundant and correlative information if we simply combine all the features into a single large feature vector.

PCA has often been used for feature length reduction to remove redundant information. However, simply using the PCA on a large feature vector combining all the individual feature vectors may not work here. In addition to the expensive computational requirement, the short feature vectors of small dimensions and scales will be overwhelmed by other long feature vectors even if the small features may contain discriminating information. To avoid this problem, we use an NMDEE for plankton feature combination and extraction.

The MDEE [14] cuts a long feature vector into sections of small vectors, and then performs a PCA on each small vector separately. The selected top features with large eigenvalues in each section are then combined to form a new feature vector with a second PCA applied again. Several orders of computation complexity reduction from the conventional PCA are achieved by this method. As illustrated in Fig. 8, the first step PCA is only applied to the LVs. Then a truncated LV (TLV) is computed by selecting only the top few eigenfeatures with the largest eigenvalues. The TLVs and SVs are then combined to form a new feature vector for the second step PCA.

The difference between the PCA and MDEE is the information that is thrown away in the second step, where only the dominant eigenfeatures in each group are kept. The discarded information is contained in three groups of covariance matrices [14].

TABLE I
COMPARISON OF THE ORIGINAL AND THE TRUNCATE LENGTH OF EACH FEATURE VECTOR

Feature Name	Original Length	Truncate Length
FD	360	2
Filled FD	360	2
P1	50	4
P2	50	4
Filled P1	50	4
Filled P2	50	3
Radon Moments	180	4

They are the covariance matrices of the removed small eigenfeatures within each group, the cross-covariance matrices between the removed small eigenfeatures of each group, and the cross-covariance matrices between the small eigenfeatures in one group and the dominant eigenfeatures in another group. Because of the energy packing property of PCA, the information in the first two types of matrices should be negligible.

We can also argue that the information in the third type of matrices cannot be large either. If two feature groups are fairly uncorrelated with each other, then any cross-covariance matrices between the two groups will be very small. On the other hand, if the two groups are strongly correlated with each other, the dominant eigenfeatures of the two groups will be very similar. Therefore the cross-covariance matrix between the dominant features in one group and the small features in another group will be similar to the cross-covariance matrix between the dominant features and the small features within the same group, which is zero due to the decorrelation property of the first step PCA transform. Since all three types of matrices are small, we conclude that the information that is discarded in the second step of MDEE is insignificant.

Because the original vector length and scale are different, the scale in the TLVs and SVs can also be very different. One may overwhelm the other. We add a normalization step to all features in the new combined feature vector to remove the effect of different scales. Notice that after the first step PCA, the scales of the TLVs not only reflect the scales of the original features but also reflect the length of the original feature vectors. Therefore, adding a normalization step here will normalize both scale and length of each of the original feature vectors. In later experiments, we will see the significance of this normalization step.

III. EXPERIMENT AND DISCUSSION

We used 3147 binary images of seven plankton classes for the experiments. Seven types of LV are extracted, including FD, filled FD (FD extracted from the boundary of the flood-filled image, the following "filled" are *the same meaning*), $P1$, $P2$, filled $P1$, filled $P2$ and CMS. Their original feature lengths are shown in Table I. Four types of SV are extracted, including Granulometry, moment invariants, boundary smoothness, and object width density. The final algorithm combines all the LVs and SVs using the NMDEE. The Gaussian minimum error classifier is adopted to classify the plankton images.

We first compute PCA on the seven LVs. Their energy distributions represented by the eigenvalues are shown in Fig. 9. We

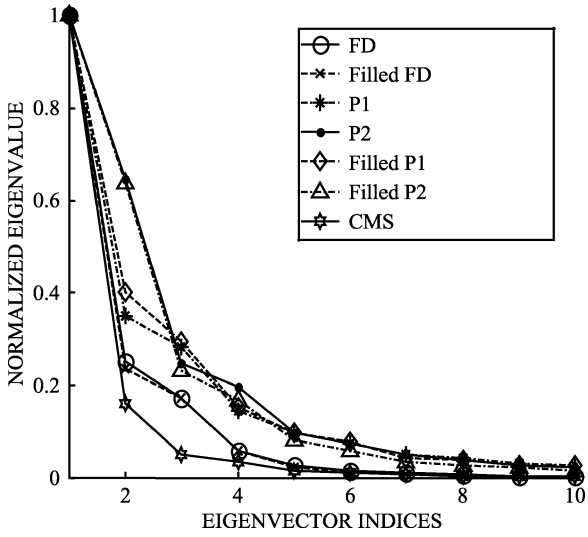

Fig. 9. Distributions of the top ten normalized eigenvalues parsed from the PCA of the seven kinds of LVs.

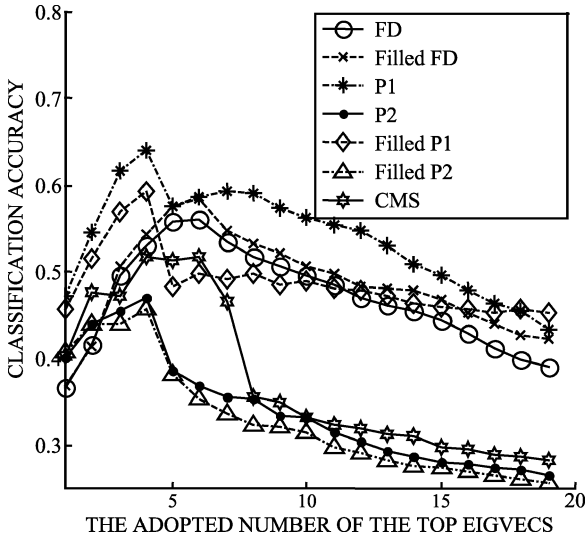

Fig. 10. Classification rates using increasing number of principal components for the seven feature vectors.

can see that most of the energy concentrates in the top 2–4 eigenvectors. Classification results using different number of eigenfeatures are shown in Fig. 10. Again, using only a small number of features the highest recognition rate is reached for the feature vector. Further increasing of feature length seems to add more noise than discriminating information, thus decreasing the recognition accuracy. Therefore, we only keep a small number of principle features in each vector as shown in Table I.

Results in Fig. 10 show that each individual feature vector is not effective to classify plankton. All classification accuracies are below 65% because of the large variations of *within-class* plankton images. Since each feature vector characterizes the shape from different aspect, the combined vector should perform better.

To illustrate the performance of NMDEE, we compare it with two traditional methods. One is traditional PCA, which extracts the principal components directly from the combination of

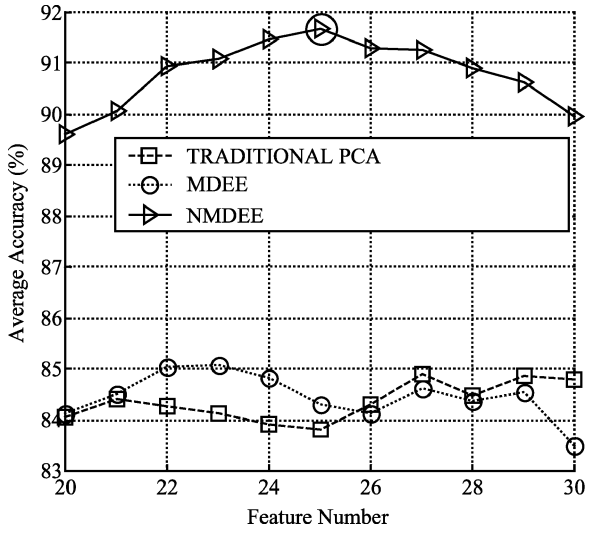

Fig. 11. Classification accuracies using combined feature vectors. The circle on the NMDEE curve marks the best accuracy of 91.7%.

TABLE II
CLASSIFICATION RESULT (CONFUSION MATRIX) OF NORMALIZED MDEE AT FEATURE NUMBER 25 (CIRCLED IN THE FIG. 11)

Class ID	1	2	3	4	5	6	7	Accuracy
1	115	0	4	4	0	8	0	87.79%
2	0	149	8	0	13	0	2	86.63%
3	3	4	415	16	9	1	2	92.22%
4	25	0	23	432	0	0	5	89.07%
5	1	6	24	0	485	1	12	91.68%
6	7	0	3	0	6	536	11	95.20%
7	2	5	5	5	19	25	728	92.27%
Average Accuracy				91.70%				

all original feature vectors. The other is the standard MDEE without the normalization process.

We combine all the long and short feature vectors using the NMDEE algorithm. Results are shown in Fig. 11. We can see a remarkable improvement of the accuracy over individual features. Over 91% accuracy is achieved. We also compare the NMDEE with standard PCA and MDEE methods. Results in Fig. 11 show that the latter two methods are very similar to each other. This is not surprising, since MDEE is a close approximation of PCA, with a significant computational complexity reduction. Both methods are much worse than the NMDEE method, since all features, large or small, can contribute to the classification using the NMDEE method. Table II shows the confusion matrix of the best performing NMDEE at feature length 25 with average accuracy 91.70%.

IV. CONCLUSION

In this paper, several new shape features are proposed to classify binary plankton images. The traditional PCA is not efficient in extracting discriminant information from a combined feature vector of different scales. A normalized MDEE is proposed to solve this problem. Experimental results on a large data set show that the new algorithm can effectively classify plankton images with high accuracy acceptable for automatic plankton survey systems.

REFERENCES

[1] C. S. Davis, S. M. Gallager, and A. R. Solow, "Microaggregations of oceanic plankton observed by towed video microscopy," *Science*, vol. 257, pp. 230–232, Jul. 10, 1992.

[2] G. L. Foresti and S. Gentilli, "Noise-robust and invariant object classification by the high-order statistical pattern spectrum," *Int. J. Pattern Recognit. Artif. Intell.*, vol. 13, no. 8, pp. 1219–1232, 1999.

[3] J. Watson, G. Craig, V. Chalvidan, J. P. Chambard, A. Diard, G. L. Foresti, B. Forre, S. Gentili, P. R. Hobson, R. S. Lampitt, P. Maine, J. T. Malmo, H. Nareid, G. Pieroni, S. Serpico, K. Tipping, and A. Trucco, "High resolution in situ holographic recording and analysis of marine organisms and particles (Holomar)," in *Proc. IEEE Int. Conf. OCEAN '98*, 1998, pp. 1599–1604.

[4] S. Samson, T. Hopkins, A. Remsen, L. Langebrake, T. Sutton, and J. Patten, "A system for high-resolution zooplankton imaging," *IEEE J. Ocean. Eng.*, vol. 26, no. 4, pp. 671–676, Oct. 2001.

[5] X. Tang, "Multiple competitive-learning network fusion for object classification," *IEEE Trans. Syst., Man, Cybern.*, vol. 28, no. 4, pp. 532–543, Aug. 1998.

[6] C. T. Zahn and R. Z. Roskies, "Fourier descriptors for plane closed curve," *IEEE Trans. Comput.*, vol. 21, no. 3, pp. 269–281, Mar. 1972.

[7] E. Persoon and K. S. Fu, "Shape discrimination using Fourier descriptors," *IEEE Trans. Syst. Man, Cybern.*, vol. 7, pp. 170–179, Mar. 1977.

[8] H. Kauppinen, T. Seppanen, and M. Pietikainen, "An experimental comparison of autoregressive and Fourier-based descriptors in 2D shape classification," *IEEE Trans. Pattern Anal. Mach. Intell.*, vol. 17, no. 2, pp. 201–207, Feb. 1995.

[9] A. P. Reeves, R. J. Prokop, S. E. Andrews, and F. P. Kuhl, "Three-dimensional shape analysis using moments and Fourier descriptors," *IEEE Trans. Pattern Anal. Mach. Intell.*, vol. 10, no. 6, pp. 937–943, Nov. 1988.

[10] M. F. Wu and H. T. Sheu, "Representation of 3D surfaces by two-variable Fourier descriptors," *IEEE Trans. Pattern Anal. Mach. Intell.*, vol. 20, no. 8, pp. 853–863, Aug. 1998.

[11] T. H. Reiss, "The revised fundamental theorem of moment invariants," *IEEE Trans. Pattern Anal. Mach. Intell.*, vol. 13, no. 8, pp. 830–834, Aug. 1991.

[12] C. H. Teh and R. T. Chin, "On image analysis by the method of moments," *IEEE Trans. Pattern Anal. Mach. Intell.*, vol. 10, pp. 496–513, Jul. 1988.

[13] S. Ghosal and R. Mehrotra, "A moment-based unified approach to image feature detection," *IEEE Trans. Image Process.*, vol. 6, no. 6, pp. 781–793, Jun. 1997.

[14] X. Tang, " Texture information in run-length matrices," *IEEE Trans. Image Process.*, vol. 7, no. 11, pp. 1602–1609, Nov. 1998.

[15] P. F. Culverhouse, R. Williams, B. Reguera, V. Herry, and S. Gonzalez-Gil, "Do experts make mistakes? A comparison of human and machine identification of dinoflagellates," *Mar. Ecology Progress Ser.*, vol. 247, pp. 17–25, 2003.

[16] G. Matheron, *Random Sets and Integral Geometry*. New York: Wiley, 1975.

[17] P. Soille and H. Talbot, "Directional morphological filtering," *IEEE Trans. Pattern Anal. Mach. Intell.*, vol. 23, no. 11, pp. 1313–1329, Nov. 2001.

[18] P. Maragos, " Pattern spectrum and multiscale shape representation," *IEEE Trans. Pattern Anal. Mach. Intell.*, vol. 11, no. 7, pp. 701–716, Jul. 1989.

[19] G. Ayala and J. Domingo, " Spatial size distributions: applications to shape and texture analysis," *IEEE Trans. Pattern Anal. Mach. Intell.*, vol. 23, no. 12, pp. 1430–1442, Dec. 2001.

[20] X. Tang, W. K. Stewart, L. Vincent, H. Huang, M. Marty, S. M. Gallager, and C. S. Davis, "Automatic plankton image recognition," *Artif. Intell. Rev.*, vol. 12, pp. 177–199, 1998.

Xiaoou Tang (S'93–M'96–SM'02) received the B.S. degree from the University of Science and Technology of China, Hefei, China, in 1990, the M.S. degree from the University of Rochester, Rochester, NY, in 1991, and the Ph.D. degree from the Massachusetts Institute of Technology, Cambridge, in 1996.

He is currently a Professor with the Department of Information Engineering, The Chinese University of Hong Kong, Hong Kong and the Group Manager of the Visual Computing Group at the Microsoft Research Asia. His research interests include video processing, computer vision, and pattern recognition.

Dr. Tang is an Associate Editor of IEEE TRANSACTIONS ON PATTERN ANALYSIS AND MACHINE INTELLIGENCE and *Pattern Recognition Journal*. He has been a Guest Editor for IEEE JOURNAL OF OCEANIC ENGINEERING and IEEE TRANSACTIONS ON CIRCUITS AND SYSTEMS FOR VIDEO TECHNOLOGY. He is the local Chair of the International Conference on Computer Vision (ICCV) 2005, an area Chair of CVPR'07, a program Chair of ICCV'09, and a general Chair of the IEEE ICCV International Workshop on Analysis and Modeling of Faces and Gestures 2005.

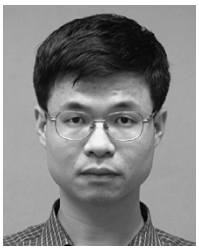

Feng Lin received the B.S. and M.S. degrees in electronic engineering from the University of Science and Technology of China, Hefei, China, in 1997 and 2000, respectively, and the Ph.D. degree in information engineering from the Chinese University of Hong Kong, Hong Kong, in 2003.

He is currently a Postdoctoral Fellow with the Department of Information Engineering, The Chinese University of Hong Kong. His research interests include pattern recognition, image processing, and computer vision.

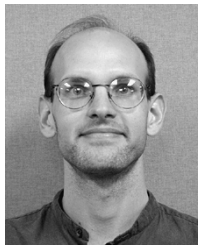

Scott Samson received the B.S.E. degree in biomedical engineering in 1990 and the Ph.D. degree in electrical engineering in 1994, from the University of Iowa, Iowa City.

He is a Sensor Engineer with the Center for Ocean Technology, University of South Florida, Tampa. His expertise includes development of microelectromechanical systems (MEMS), integrated optics, imaging, and electronic systems. He previously worked in industry as a research engineer, developing electrooptic modulators for military and commercial applications. His interests include the development of improved and miniaturized optoelectronic sensors for deployment in the marine environment.

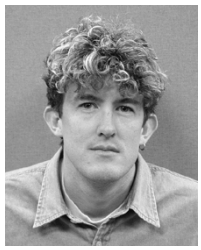

Andrew Remsen received the B.S. degree in biology from the University of Wisconsin, Madison, in 1991 and he is currently working towards the Ph.D. degree in biological oceanography at the College of Marine Science, University of South Florida. Tampa.

His interests include software and sensor development, the small-scale distribution of particles in the ocean, and the effect of large rivers on tropical ocean systems.